

# On Nature of Bound and Resonance States in $^{12}\text{C}$

V. S. Vasilevsky<sup>a</sup>, F. Arickx<sup>b</sup>, W. Vanroose<sup>b</sup>  
and J. Broeckhove<sup>b</sup>

<sup>a</sup>*Bogolyubov Institute for Theoretical Physics, Kiev, Ukraine*

<sup>b</sup>*Departement Wiskunde-Informatica, Universiteit Antwerpen, Antwerpen, Belgium*

## Abstract

We investigate both bound and resonance states in  $^{12}\text{C}$  embedded in a three- $\alpha$ -cluster continuum using a three-cluster microscopic model. The model relies on the Hyperspherical Harmonic basis to enumerate channels describing the three-cluster discrete and continuous spectrum states. It yields the most probable distribution of three  $\alpha$ -clusters in space, and the dominant decay modes of the three-cluster resonances.

**Keywords:** *Cluster model; resonance state; Hoyle state; hyperspherical harmonics*

## 1 Introduction

The  $^{12}\text{C}$  nucleus is an interesting example of the so-called Borromean nuclei as it has no bound states in any two-cluster subsystem of its three-cluster configuration. The lowest dissociation threshold (7.276 MeV above the ground state) is that of a three  $\alpha$  particles disintegration. This three-cluster configuration is thus responsible to a great extent for the formation of a few bound and many resonance states. The next threshold is of a two-cluster nature:  $^{11}\text{B} + p$  [1]. It opens when the excitation energy of  $^{12}\text{C}$  exceeds 15.96 MeV. One therefore expects only a negligible influence of the latter channel on bound and resonance states of  $^{12}\text{C}$  in the vicinity of the  $\alpha + \alpha + \alpha$  threshold.

The  $^{12}\text{C}$  nucleus is unique because of its excited “Hoyle state”. This state is important in the context of nucleosynthesis of carbon in helium-burning red giant stars. It is a  $0^+$  state with an energy of 7.65 MeV above the ground state, or 0.4 MeV above the three-cluster  $\alpha + \alpha + \alpha$  threshold. Its width is only 8.5 eV indicating a long lifetime. One immediately relates this to the  $0^+$  state in  $^8\text{Be}$  described by two  $\alpha$  particles with an energy of 0.092 MeV above the  $\alpha + \alpha$  threshold and a width of 5.57 eV.

Many efforts have been made to reproduce the experimentally observed structure of  $^{12}\text{C}$  and to explore and understand the nature of the ground, excited and resonance states. This was, for example, done within so-called semi-microscopic models (considering structureless  $\alpha$ -particles) [2–8] and within fully microscopic models [9–24].

A somewhat general feature of the calculations is that, with potentials which adequately reproduce the  $\alpha$ - $\alpha$  interaction (this includes the phase shifts for  $0^+$ ,  $2^+$  and  $4^+$  states and the position of the corresponding resonance states), one obtains a noticeably overbound ground state for  $^{12}\text{C}$ .

To determine the energies and widths of resonance states created by a three-cluster continuum, only a few methods can be used. A popular method for obtaining the resonance properties in many-cluster, many channel systems is the Complex Scaling Method (see reviews [25, 26] and references therein). Other methods start from a calculated form of the  $S$ -matrix in a wide energy range and determine the resonance states as the pole(s) of the  $S$ -matrix. The advantage of these methods is that they provide the scattering quantities (such as phase-shifts, cross-sections, etc.) and the resonance properties (energies and widths), as well as the wave functions of scattering

and resonance states. The latter then allow one to obtain more information about the nature of the resonance states.

$^{12}\text{C}$  is known from theory and experiment (see, e. g., [27] and [28]) to have very narrow resonances above the three  $\alpha$  threshold. One may wonder why a system with several open channels does not decay instantly but manifests these narrow resonance states. There are two possible answers to this question. First, a resonance state appears in one single channel of the multi-channel system. Such particular channel is usually weakly coupled to a number, or all, of the other open channels. It is well-known that this weak coupling of channels predetermines the existence of long-lived resonance states. Second, a resonance can be more or less uniformly distributed over all open channels, and the compound system needs (some) time for the resonance to be accumulated by one or a few open channels to decay into. Such a distribution over many open channels leads to very narrow resonances, as was predicted by A. Baz' [29]. It is referred to as diffusion-like processes in scattering. This type of resonance is attributed to the effect that “the system spends most of its time wandering from one channel to another” [29].

In this paper we wish to calculate and analyze the bound and continuum structure of  $^{12}\text{C}$ , and gain some insight in the nature of these states. Indeed, in some publications (e. g., [30–33]) the suggestion for a dominant linear, chain-like, three-cluster structure appears for some of the  $^{12}\text{C}$  resonances. We will look for a confirmation of this structure. To this end, we determine the most probable configuration of three  $\alpha$  particles both in coordinate and momentum space. We also qualify the channels through which the resonance states of  $^{12}\text{C}$  preferentially decay.

The main results of this paper are obtained by applying the “Algebraic Model in a Hyperspherical Harmonic Basis” (AMHHB) [34, 35, 36] to a configuration of three  $\alpha$  particles. In this model, the three clusters are treated equally and their relative motion is described by Hyperspherical Harmonics. The latter enumerate the channels of the three-cluster continuum and allow one to implement the correct boundary conditions for the three-cluster exit channels. The AMHHB has been applied successfully to a study of resonances in nuclei with a large excess of protons or neutrons such as  $^6\text{He}$ ,  $^6\text{Be}$ ,  $^5\text{H}$ . The method provides energies and widths of resonances and their total and partial widths, as well as the corresponding wave functions. The latter allow one to analyze the nature of the resonance states. The results of this model are compared to those obtained in other, more or less comparable, microscopic descriptions from the literature and to experiment.

In the next section we elaborate the method used to calculate the spectrum of  $^{12}\text{C}$ . Section three focuses on the results obtained using this method. We also present correlation functions and density functions to characterize more precisely the spatial configuration of the three  $\alpha$  particles for specific resonance states. We also compare the results to those of other microscopic calculations as well as to experiment.

## 2 Microscopic cluster model

In this section we describe the microscopic model used to determine the structure of  $^{12}\text{C}$  in the present paper. As it has been already introduced and used in several publications, we will limit ourselves to the most important notations and aspects of importance to the current calculations.

### 2.1 Three-cluster AMHHB model

The three-cluster “Algebraic Model in a Hyperspherical Harmonic Basis” (AMHHB) [34–36] will be applied to a single  $^{12}\text{C} = \alpha + \alpha + \alpha$  three-cluster configuration.

This model takes a Hyperspherical Harmonic basis (HH) to characterize and enumerate different three-cluster channels. In each of these channels, an oscillator basis

describes the radial behavior and is used to expand the many-particle wave function. A matrix version of the Schrödinger equation is obtained after substitution of this wave function. It is solved by the Algebraic Method (also called the Modified  $J$ -Matrix method [36]) for both bound and scattering states using the correct asymptotics.

A similar approach utilizing the Hyperspherical Harmonics, was proposed in [38, 39] in the coordinate representation using the generator coordinate technique to solve the corresponding Schrödinger equation.

The AMHHB wave function for  $^{12}\text{C}$  is written as

$$\begin{aligned}\Psi &= \widehat{\mathcal{A}}\{\Phi(\alpha_1)\Phi(\alpha_2)\Phi(\alpha_3)f(\mathbf{x},\mathbf{y})\} \\ &= \widehat{\mathcal{A}}\{\Phi(\alpha_1)\Phi(\alpha_2)\Phi(\alpha_3)f(\rho,\theta;\widehat{\mathbf{x}},\widehat{\mathbf{y}})\} \\ &= \sum_{n_\rho,K,l_1,l_2} C_{n_\rho,K,l_1,l_2} |n_\rho,K,l_1,l_2;LM\rangle(\rho,\theta;\widehat{\mathbf{x}},\widehat{\mathbf{y}}),\end{aligned}\quad (1)$$

where  $|n_\rho,K,l_1,l_2;LM\rangle$  is a cluster oscillator function [34]:

$$|n_\rho,K,l_1,l_2;LM\rangle = \widehat{\mathcal{A}}\{\Phi(\alpha_1)\Phi(\alpha_2)\Phi(\alpha_3)R_{n_\rho,K}(\rho)\chi_{K,l_1,l_2}(\theta)\{Y_{l_1}(\widehat{\mathbf{y}})Y_{l_2}(\widehat{\mathbf{x}})\}_{LM}\}.\quad (2)$$

These functions are labelled by the number of hyperradial excitations  $n_\rho$ , hyperspherical momentum  $K$  and two partial orbital momenta  $l_1, l_2$ . The vectors  $\mathbf{x}$  and  $\mathbf{y}$  form a set of Jacobi coordinates, and  $\rho$  and  $\theta$  are hyperspherical coordinates related to the Jacobi vectors by:

$$\rho = \sqrt{\mathbf{x}^2 + \mathbf{y}^2}, \quad |\mathbf{x}| = \rho \cos \theta, \quad |\mathbf{y}| = \rho \sin \theta.\quad (3)$$

The notation  $\widehat{\mathbf{x}}$  and  $\widehat{\mathbf{y}}$  refers to the unit length vectors. The vector  $\mathbf{x}$  corresponds to the distance between two selected  $\alpha$  particles with the associated partial orbital angular momentum  $l_2$ . The vector  $\mathbf{y}$  is the displacement of the third  $\alpha$  particle with respect to the center of mass of two others with the associated angular momentum  $l_1$ . The three quantum numbers  $c = \{K, l_1, l_2\}$  determine channels of the three-cluster system in the AMHHB.

The fact that all three clusters are identical leads to some specific issues. The wave function (1) for  $^{12}\text{C}$  is antisymmetric with respect to the permutation of any pair of nucleons. Because the three clusters are identical, this function should be symmetric with respect to the permutation of any pair of alpha particles. This imposes constraints on the allowed quantum numbers of the wave function. Because of this symmetry, for instance, the partial orbital momentum  $l_2$  of a two-cluster subsystem can only have even values. As the parity of  $^{12}\text{C}$  states is defined as  $\pi = (-1)^{l_1+l_2}$ , it is fully determined by the partial orbital angular momentum  $l_1$  of the relative motion of the remaining cluster with respect to the two-cluster subsystem.

It was suggested in Refs. [40] and [12] to use a symmetrization operator to construct the proper basis states. For a discussion on the symmetry of a system with three identical clusters we refer to [41].

The symmetrical Hyperspherical Harmonic basis for a three-particle system was realized many years ago (see, e. g., [42, 43]). An explicit form of a few basis functions for small values of the total orbital momentum ( $L = 0, 1$  and  $2$ ) can be derived. However it is extremely intricate to use for explicit calculation of matrix elements.

An alternative approach to obtain such matrix elements without an explicit realization of the basis functions consists in using the generating function technique. One can indeed construct a generating function for the overlap and Hamiltonian kernels of  $^{12}\text{C}$  using the procedure explained in [34] that satisfies all required symmetry conditions including the cluster symmetric permutation behavior. Explicit matrix elements of the operators can then be obtained by using recurrence relations. The standard

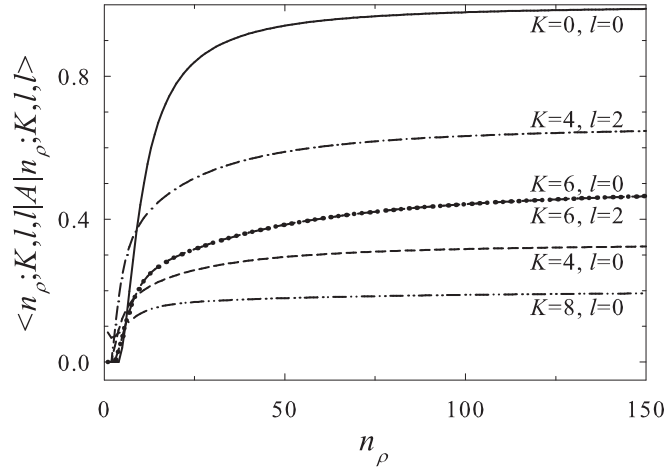


Figure 1: Matrix elements of the antisymmetrization operator in the nonsymmetrized hyperspherical basis ( $K = 6, l = 0$  and  $K = 6, l = 2$  coincide).

approach in the AMHHB is to extract matrix elements characterized by explicit  $l_1, l_2$  quantum numbers. These, however, do not yet correspond to the desired symmetrical Harmonics. Indeed, the states  $|n_\rho, K, l_1, l_2; LM\rangle$  for fixed  $n_\rho$  and  $K$  do not belong to the desired symmetrical irreducible representation of  $S(3)$ , the permutation group of the three  $\alpha$  clusters, with the Young tableau [3]. They are, in fact, linear combinations of the Young tableau [3] and the non-symmetrical Young tableaux [2,1] and [111].

The antisymmetrization operator in the standard AMHHB basis has non-zero matrix elements

$$\langle n_\rho, K, l_1, l_2; LM | \hat{A} | \tilde{n}_\rho, \tilde{K}, \tilde{l}_1, \tilde{l}_2; LM \rangle \quad (4)$$

for fixed oscillator shells with  $N_{sh} = 2n_\rho + K = 2\tilde{n}_\rho + \tilde{K}$ . By selecting only matrix elements with hyperradial quantum number  $n_\rho = \tilde{n}_\rho$  and hypermomentum  $K = \tilde{K}$ , one obtains relatively small matrices whose eigenfunctions  $|n_\rho, K, \nu; LM\rangle$  with non-zero eigenvalues are of the correct symmetrical hyperspherical type due to the symmetry properties of the generating function. Index  $\nu = 1, 2, \dots$  enumerates the symmetrical Hyperspherical Harmonics for a given value of the hypermomentum  $K$ . This procedure is similar to the procedure of obtaining Pauli allowed states in three-cluster systems (see Ref. [44] for details).

This is demonstrated in Fig. 1 where the diagonal matrix elements of the antisymmetrization operator between the original Hyperspherical Harmonics are displayed for total orbital momentum  $L = 0$  for all channels up to  $K = 8$ . One notices that matrix elements

$$\langle n_\rho, K, l_1 = l_2; L = 0 | \hat{A} | n_\rho, K, l_1 = l_2; L = 0 \rangle \quad (5)$$

do not tend to unity, as one could expect, but to some fixed values. Analysis shows that these asymptotic values of (5) correspond to the weights of the symmetrized Hyperspherical Harmonics with Young tableau [3], within the original Harmonic.

The eigenvalues obtained after diagonalization which are matrix elements of symmetrized Harmonics, however, do display the correct asymptotic behavior, i. e. they all tend to unity as can be seen in Fig. 2.

In Table 1, we display both the total number of (original) nonsymmetrized and of symmetrized channels for different values of the total orbital momentum. The symmetrization significantly reduces the number of channels compatible with the maximal value of hypermomentum  $K_{\max}$ . Only even values of the partial orbital momentum  $l_2$  are considered because of the symmetry rules for two-cluster subsystems.

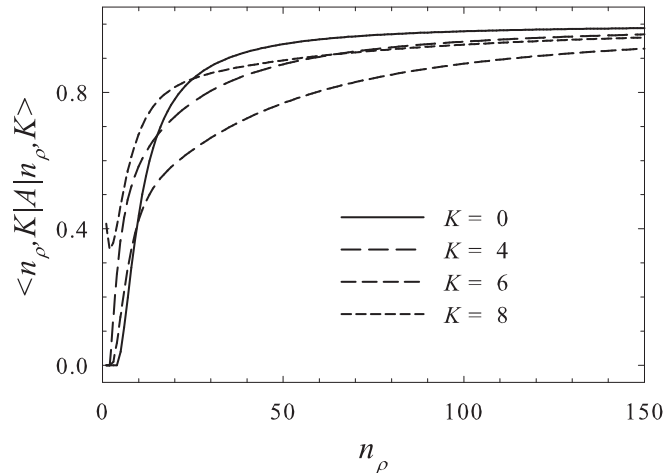


Figure 2: Matrix elements of the antisymmetrizer in the symmetrized hyperspherical basis.

Table 1: Number of channels for nonsymmetrized and symmetrized Hyperspherical Harmonics (enumerated by  $\nu$  for given  $K$ ).

$J^{\pi}$	$0^+$	$2^+$	$4^+$	$1^-$	$3^-$
$K_{\max}$	14	14	14	13	13
$N_{ch}(\{K, l_1, l_2\})$	20	44	54	28	42
$N_{ch}(\{K, \nu\})$	8	16	19	9	14

Effective charges  $Z_{c,\tilde{c}}$  were defined in Refs. [34] and [35] in the context of the AMHHB and their importance and meaning were explicitly discussed for the  $^6\text{Be}$  nucleus in the three-cluster configuration  $^4\text{He} + p + p$ . The effective charge determines the asymptotic form of the three-cluster potential originating from the Coulomb interaction, which has the form

$$V_{c,\tilde{c}}^{(C)} = \frac{Z_{c,\tilde{c}}}{\rho}. \quad (6)$$

It was shown that it is of a crucial importance for implementing the correct boundary conditions for the three-cluster continuum states.

The symmetrization influences the behavior of the effective charges. In Table 2, we display the effective charges for the  $0^+$  state of  $^{12}\text{C}$  calculated in the original

Table 2: Effective charges for the  $J^{\pi} = 0^+$  state of  $^{12}\text{C}$ .

$(K, l_1, l_2)$	(0,0,0)	(4,0,0)	(4,2,2)	(6,0,0)	(6,2,2)	(8,0,0)	(8,2,2)	(8,4,4)
(0,0,0)	28.81	2.47	3.49	2.74	-2.74	0.87	0.00	1.04
(4,0,0)	2.47	32.157	-1.13	3.95	-0.31	4.67	0.00	1.95
(4,2,2)	3.49	-1.13	31.35	1.72	-4.30	0.00	0.66	0.00
(6,0,0)	2.74	3.95	1.72	33.48	-2.51	4.63	0.00	0.45
(6,2,2)	-2.74	-0.31	-4.30	-2.51	34.29	0.00	0.62	0.00
(8,0,0)	0.87	4.67	0.00	4.63	0.00	34.29	0.00	-2.38
(8,2,2)	0.00	0.00	0.66	0.00	0.62	0.00	33.08	0.00
(8,4,4)	1.04	1.95	0.00	0.45	0.00	-2.38	0.00	32.41

Table 3: Effective charges for the  $J^\pi = 0^+$  state of  $^{12}\text{C}$  for symmetrized channels.

$(K, \nu)$	(0,1)	(4,1)	(6,1)	(8,1)
(0,1)	28.810	4.277	3.880	1.139
(4,1)	4.277	30.556	5.217	2.301
(6,1)	3.880	5.217	35.990	1.457
(8,1)	1.139	2.301	1.457	31.450

nonsymmetrized basis of the Hyperspherical Harmonics for  $K_{max} = 8$ . One easily verifies that they coincide with those calculated in [23].

We display the effective charges in the symmetrized basis in Table 3. Only four channels remain after symmetrization. In particular, no  $K = 2$  channel remains, so, we omitted these also in Table 2 even though they have a non-zero contribution.

It goes without saying that the asymptotic form of the effective three-cluster potential which originates from the nucleon-nucleon interaction [34],

$$V_{c,\tilde{c}}^{(NN)} = \frac{V_{c,\tilde{c}}}{\rho^3}, \quad (7)$$

is also influenced by the symmetrization. This asymptotic component is very important for obtaining the correct values of the  $S$ -matrix. We do not dwell on its explicit form here but apply a procedure similar to that for the effective charges.

## 2.2 Phases, eigenphases and resonances

After solving the system of linear equation of the AMHHB model, we obtain the wave functions of continuous spectrum states and the scattering  $S$ -matrix. We consider two different representations of the  $S$ -matrix.

In the first representation, the elements of the  $S$ -matrix are described through the phase shifts  $\delta_{ij}$  and inelastic parameters  $\eta_{ij}$ ,

$$S_{ij} = \eta_{ij} \exp(2i\delta_{ij}), \quad (8)$$

of which one usually analyzes only the diagonal matrix elements by displaying the  $\delta_{ii}$  and  $\eta_{ii}$  quantities. In the second representation, the  $S$ -matrix is reduced to the diagonal form leading to the so-called eigenphases which now represent the elastic scattering of the many-channel system in terms of independent (uncoupled) eigenchannels:

$$\|S\| = \|U\|^{-1} \|D\| \|U\|. \quad (9)$$

Here  $\|U\|$  is an orthogonal matrix relating both representations, and  $\|D\|$  is a diagonal matrix with nonzero elements

$$D_{\alpha\alpha} = \exp(2i\delta_\alpha) \quad (10)$$

defining the eigenphases  $\delta_\alpha$ .

The phases shifts  $\delta_{ii}$ , inelastic parameters  $\eta_{ii}$  and eigenphases  $\delta_\alpha$  provide a sufficiently detailed information about the channels that are involved in production of resonance states. The eigenphases are used to extract resonance positions and total widths in a traditional way:

$$\left. \frac{d^2\delta_\alpha}{dE^2} \right|_{E=E_r} = 0, \quad \Gamma = 2 \left( \left. \frac{d\delta_\alpha}{dE} \right|_{E_r} \right)^{-1}; \quad (11)$$

whereas the orthogonal matrix  $\|U\|$  leads to the partial decay widths of the resonance (see, e. g., Ref. [36] for details).

### 2.3 Correlation functions and density distributions.

As we have pointed out, the AMHHB model allows one not only to calculate the scattering observables but also to obtain the wave function at any energy, in particular, at the resonance. The latter is of the utmost importance for the analysis of the nature of the system at these energies.

Within the AMHHB model, the solution is fully expressed by the expansion coefficients  $\{C_{n_\rho,c}\}$  and the  $S$ -matrix. The expansion coefficients  $\{C_{n_\rho,c}\}$  determine both the total three-cluster wave function of a compound system  $\Psi$  as well as the wave function of the relative motion of three clusters  $f(\mathbf{x}, \mathbf{y})$  (see eq. (1)).

The latter contains all information on the dynamic behavior of the three-cluster system in bound states and continuum as well. It is interesting to note that these coefficients are identical in representations of the wave function both in coordinate and momentum space because of the Fourier transform properties of the oscillator states. The wave function  $f(\mathbf{k}, \mathbf{q})$  in momentum space has arguments that are directly related to the coordinate representation:  $\mathbf{k}$  is the momentum of relative motion of two clusters, whereas  $\mathbf{q}$  is the momentum of the third cluster with respect to the center of mass of the two-cluster subsystem.

We obtain the density distribution in the coordinate space as

$$D(x, y) = D(\rho, \theta) = \int |f(\mathbf{x}, \mathbf{y})|^2 d\hat{\mathbf{x}} d\hat{\mathbf{y}}, \quad (12)$$

and the corresponding correlation function as

$$C(x, y) = C(\rho, \theta) = x^2 y^2 \int |f(\mathbf{x}, \mathbf{y})|^2 d\hat{\mathbf{x}} d\hat{\mathbf{y}} \quad (13)$$

directly from the wave function of relative motion  $f(\mathbf{x}, \mathbf{y})$ . Both the density distribution and correlation function in the momentum space are obtained in the same way using the wave function of relative motion in momentum space  $f(\mathbf{k}, \mathbf{q})$ .

In a calculation with  $N_{ch}$  open channels, one obtains  $N_{ch}$  independent wave functions describing elastic and inelastic processes in the many-channel system. It is quite impossible to analyze all of these wave functions when many channels are open. Some principles have to be set up on how to select the most important wave functions. We have formulated some criteria for selecting the dominant wave function of a resonance in Ref. [36]. We will use the same criteria in this paper to select the ‘‘resonance wave functions’’.

## 3 Calculations and results

In the present calculations for  $^{12}\text{C}$ , we consider the Minnesota potential [45] for the nucleon-nucleon interaction. The oscillator basis is characterized by the oscillator length  $b = 1.2846$  fm to minimize the ground state energy of the  $\alpha$  particle using the above potential.

The parameter  $u$  of the Minnesota potential is taken to be  $u = 0.94$  to reproduce the phase shifts of  $\alpha + \alpha$  scattering and the  $0^+$ ,  $2^+$  and  $4^+$  resonances in  $^8\text{Be}$ . The same parameters were used by Arai [17].

The  $^8\text{Be} = \alpha + \alpha$  two-cluster substructure is of a key importance in the description of  $^{12}\text{C}$ . We present  $\alpha + \alpha$  resonance properties in Table 4. The AMOB model (Algebraic Model using an Oscillator Basis) takes a set of oscillator functions to describe the intercluster behavior and the Algebraic Model to obtain the phase shifts for  $\alpha + \alpha$  scattering (see, e. g., Ref. [46]). We include a comparison to the results of Arai from his paper on  $^{12}\text{C}$  [17] where he uses the ‘‘analytical continuation of the  $S$ -matrix to the complex plane’’ method to obtain the resonance characteristics.

Table 4: Resonance properties of  ${}^8\text{Be}$  obtained with different methods.

$J^\pi$	AMOB		Arai [17]	
	$E$ , MeV	$\Gamma$ , keV	$E$ , MeV	$\Gamma$ , MeV
$0^+$	0.022	$6.30 \cdot 10^{-10}$	0.03	$<10^{-6}$
$2^+$	2.93	1.51	2.9	1.4
$4^+$	12.55	5.01	12.5	4.8

These results form a first test of the consistency of the different expansion methods applied to the two-cluster subsystem. Although quite similar, one still notices that the resonance properties of the two-cluster  $\alpha$ - $\alpha$  system have a slight dependence on the method.

### 3.1 Potential and Coulomb interaction in AMHHB

Diagonal matrix elements of the nucleon-nucleon and Coulomb interactions within the AMHHB model are displayed in Figs. 3 and 4 for the channels up to  $K = 8$ . One observes that the nucleon-nucleon interaction creates a deep potential well with a long tail in the hyperspherical coordinate. This tail reflects the asymptotic form of the potential indicated in Eq. (7). The matrix elements of the Coulomb interaction indicate the magnitude of the Coulomb barrier which is the main factor for generating resonance states in  ${}^{12}\text{C}$ .

### 3.2 Phase shifts and eigenphases

We show in Fig. 5 the results of the AMHHB calculations for the  $2^+$  state in terms of the symmetrical Hyperspherical Harmonic channels through the (diagonal) phase shifts  $\delta_{ii}$  and inelastic parameters  $\eta_{ii}$ .

The scattering parameters are obtained from a calculation with maximal hypermomentum  $K_{\max} = 14$ . One observes from Fig. 5 that for small energies the channels are completely uncoupled ( $\eta_{ii} \approx 1$ ). The first  $2^+$  resonance appears at  $E = 2.731$  MeV and is mainly produced in the first channel with the hypermomentum  $K = 2$ , whereas the second resonance at energy  $E = 3.113$  MeV is dominated by the hypermomentum  $K = 4$ . The inelastic parameters for the first two channels have pronounced

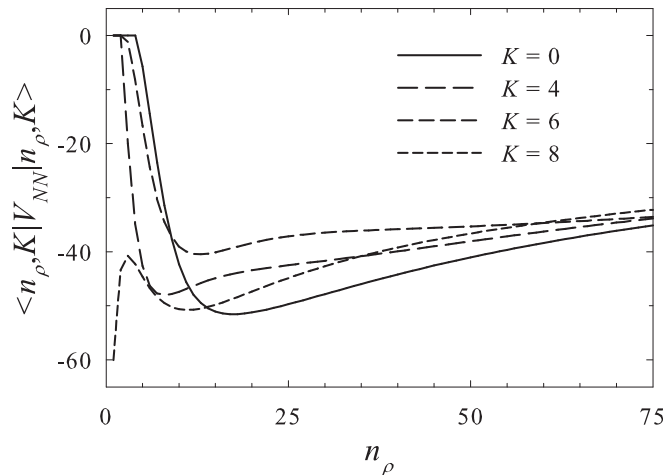


Figure 3: Diagonal matrix elements of  $\widehat{V}_{NN}$  between symmetrized Hyperspherical Harmonics for the  $J^\pi = 0^+$  state.



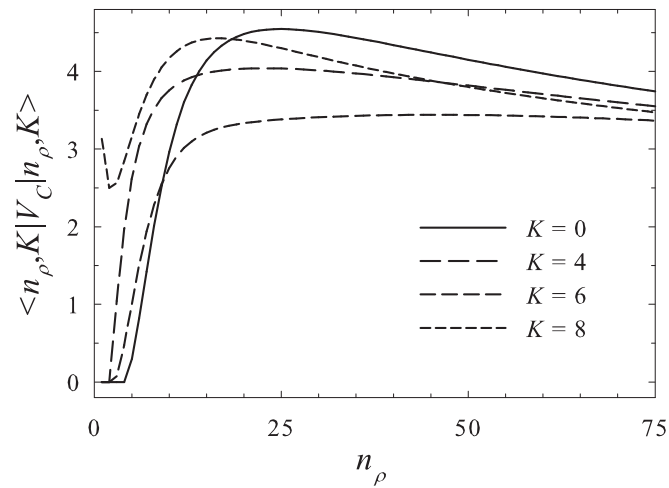


Figure 4: Diagonal matrix elements of  $\widehat{V}_C$  between symmetrized Hyperspherical Harmonics for the  $J^\pi = 0^+$  state.

minima at the energy of the first resonance and shallow minima at the second resonance energy. Besides, the first resonance displays a “shadow resonance” behavior in the second channel. This is typical for resonances in a many-channel system (see, for instance, a detailed analysis of two-channel resonances in  $^5\text{He}$  in Ref. [47]). The minima of inelastic parameters indicate that the compound system is being reconstructed at this energy and transits from one channel to the other.

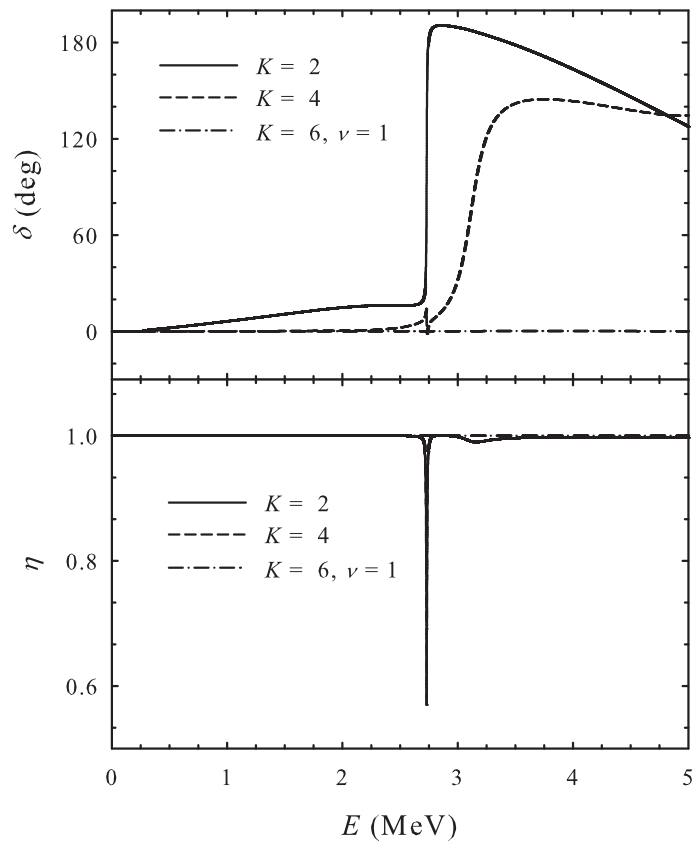


Figure 5: Diagonal phase shifts and inelastic parameters for the  $J^\pi = 2^+$  state.

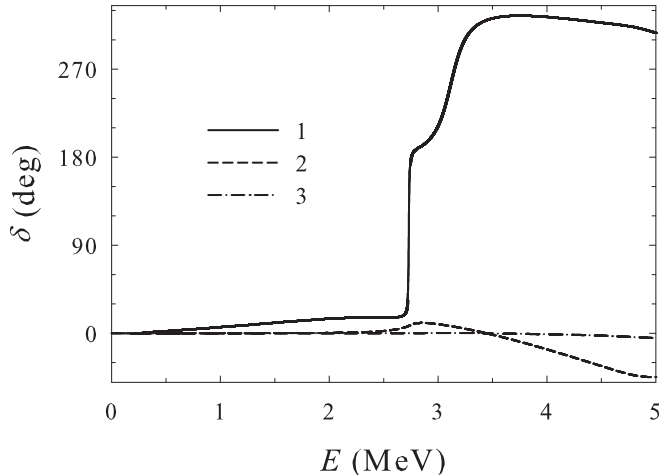


Figure 6: Eigenphase shifts for  $J^\pi = 2^+$  for the first three eigenchannels.

We display in Fig. 6 the respective eigenphase shifts  $\delta_\alpha$  for the first three eigenchannels. One observes now that both resonance states are mainly associated with the first eigenchannel while the second eigenchannel contributes only marginally.

### 3.3 Convergence properties

A convergence study of energies (and widths) of bound and resonance states should indicate whether the Hilbert space is sufficiently large for obtaining stable and reliable results. The AMHHB model space is characterized by two parameters: the maximal value of the hypermomentum  $K_{\max}$  and the maximal value of the hyper-radial excitation  $n_{\rho_{\max}}$ . Usually the choice of parameters is a compromise between the convergence of the results and the computational burden. A set of Hyperspherical Harmonics with  $K_{\max} = 14$  for even parity states and  $K_{\max} = 13$  for odd parity states, seems sufficient and remains computationally feasible. This choice accounts for a large number of three-cluster configurations or, in other words, for a sufficient number of inherent (triangular) shapes for three clusters. We refer to Ref. [48] for examples of the most probable triangular shapes associated with the Hyperspherical Harmonics with hypermomentum ranging from  $K = 0$  to  $K = 10$ .

The first convergence test considers the energies of  $0^+$ ,  $2^+$  and  $4^+$  bound states of  $^{12}\text{C}$  shown in Fig. 7 as functions of  $K_{\max}$ . One observes that the deeply bound states ( $J^\pi = 0^+$ ,  $2^+$ ) require significantly less Hyperspherical Harmonics for a converged energy than the shallow, or weakly bound, state with  $J^\pi = 4^+$ . At least all Hyperspherical Harmonics with  $K_{\max} \geq 6$  are required to bind the latter state, whereas the  $J^\pi = 0^+$  one already obtains binding with a single Hyperspherical Harmonic with  $K = 0$ . Figure 7 demonstrates also that the above choice of  $K_{\max}$  is amply sufficient for bound states.

We turn to the energies and widths of the  $0^+$  and  $2^+$  resonances obtained with increasing number of Hyperspherical Harmonics in Table 5. One observes that a sufficient convergence of the resonances occurs at  $K_{\max} = 12$ . It is furthermore interesting to note that these resonances already appear with reasonable energy and width values when only the lowest channel ( $K = 0$  for the  $0^+$  and  $K = 2$  for the  $2^+$  state) is considered. This is a remarkable result for  $^{12}\text{C}$  as, e. g., for  $^6\text{Be}$  it was impossible to generate a  $0^+$  resonance with a single  $K = 0$  channel (see Ref. [35]).

In all calculations we considered states with hyperradial excitation up to  $n_{\rho_{\max}}=70$  which cover a wide range of intercluster distances and go far enough into the asymptotic region.

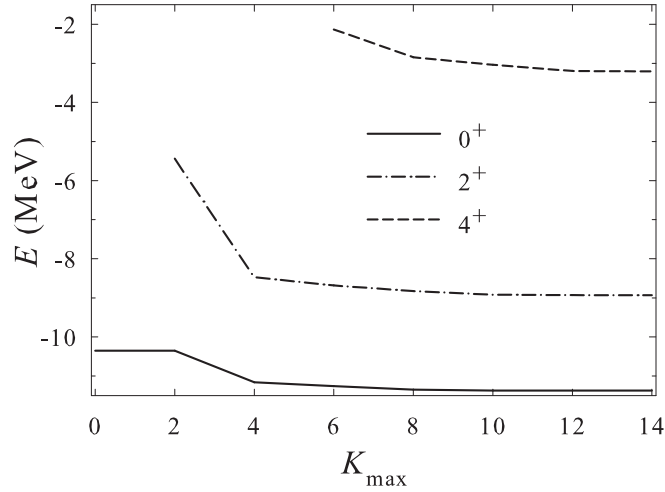


Figure 7: Convergence of bound states in AMHHB.

Table 5: Energy (MeV) and width (keV) of the low-lying resonances obtained with various  $K_{\max}$  truncations.

$J^\pi$	$K_{\max}$	0	4	6	8	10	12	14
$0^+$	$E$	0.40	0.75	0.74	0.72	0.70	0.68	0.68
	$\Gamma$	205.08	13.40	11.79	7.10	4.35	2.71	2.78
$0^+$	$E$	1.15	7.34	6.09	5.55	5.54	5.16	5.14
	$\Gamma$	510.16	897.64	422.50	539.21	586.08	534.33	523.46
$2^+$	$E$	—	3.28	2.89	2.83	2.78	2.74	2.73
	$\Gamma$	—	30.19	13.07	11.85	9.95	8.84	8.75
$2^+$	$E$	—	3.50	3.27	3.22	3.17	3.14	3.11
	$\Gamma$	—	274.51	351.57	308.29	280.23	263.80	246.78

### 3.4 Partial widths

We display the energy  $E$ , total width  $\Gamma$  and partial widths  $\Gamma_i$ ,  $i = 1, 2, \dots$  in the corresponding decay channels of the even parity resonances in Table 6 and of the odd parity resonances in Table 7.

One observes that in most cases only one or two channels are responsible for the decay of resonance states. The remaining channels contribute negligibly, and the corresponding partial widths do not exceed  $10^{-5}$  keV. A significant distribution over multiple channels is apparent only in the case of the  $4^+$  resonance.

One should note that although the resonances are created by only a few channels, the role of other very weakly coupled channels is still important. This can be seen from

Table 6: Partial widths of even parity resonances in  $^{12}\text{C}$ . Energy is in MeV, widths are in keV.

$J^\pi$		$0^+$	$2^+$	$2^+$	$4^+$
$E$		0.68	2.78	3.17	5.60
$\Gamma$		2.78	9.95	280.24	0.55
$\Gamma_1$	$K = 0$	2.78	$K = 2$ 6.11	$K = 2$ 13.46	$K = 4$ 0.23
$\Gamma_2$	$K = 4$	0	$K = 4$ 3.84	$K = 4$ 278.89	$K = 6$ 0.15
$\Gamma_3$	$K = 6$	0	$K = 6$ $<10^{-5}$	$K = 6$ $<10^{-5}$	$K = 8$ 0.16

Table 7: Partial widths of odd parity resonances in  $^{12}\text{C}$ . Energy is in MeV, widths are in keV.

$J^\pi$	$1^-$		$3^-$	
$E$		3.52		0.67
$\Gamma$		0.21		8.34
$\Gamma_1$	$K = 3$	0.206	$K = 3$	8.34
$\Gamma_2$	$K = 5$	0.002	$K = 5$	0
$\Gamma_3$	$K = 7$	$<10^{-5}$	$K = 7$	0

Table 5 for the first  $0^+$  resonance: it is indeed generated mainly by the channel with the minimal hypermomentum  $K = 0$  but is modified substantially with increasing number of hypermomenta. The same applies to other resonance states.

### 3.5 Correlation functions and density distributions.

We show the correlation function for the  $^{12}\text{C}$  ground state in Fig. 8 and observe that this state displays a compact spatial configuration, as it is expected for such a deeply bound state. The most probable shape of the three  $\alpha$ -cluster system is an almost equilateral triangle with a distance between any two  $\alpha$ -particles of approximately 3 fm.

The correlation function for the first  $0^+$  resonance state shown in Fig. 9, on the other hand, shows a more deformed system with two  $\alpha$ -particles relatively close to each other (about 3.5 fm) and the third alpha-particle located further away (approximately at a distance of 5 fm). So,  $^{12}\text{C}$  features a prolate triangle as a dominant configuration in this state.

One also observes in Fig. 9 a small maximum of the correlation function corresponding to an almost linear configuration of three  $\alpha$ -particles, two of them being approximately 4 fm apart, and the third one is located 0.2 fm away from their center of mass. However, the weight of this linear configuration is approximately 6 times less

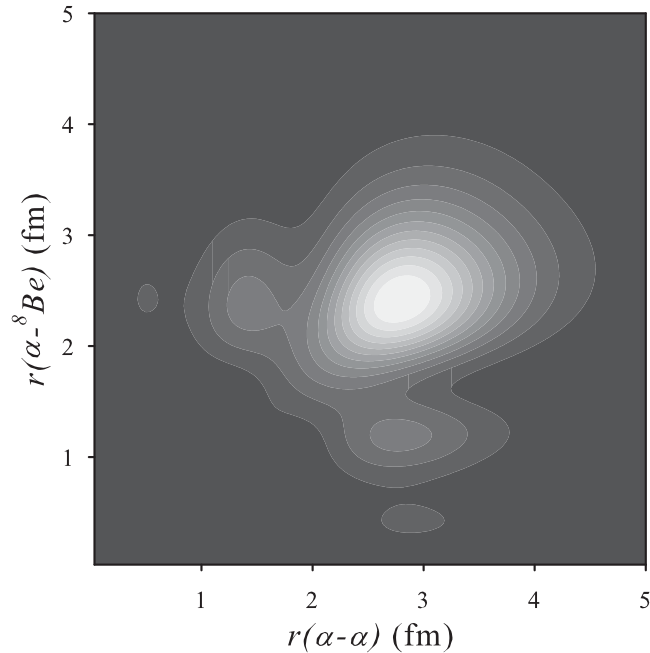


Figure 8: Correlation function for the  $^{12}\text{C}$  ground state in the coordinate space.

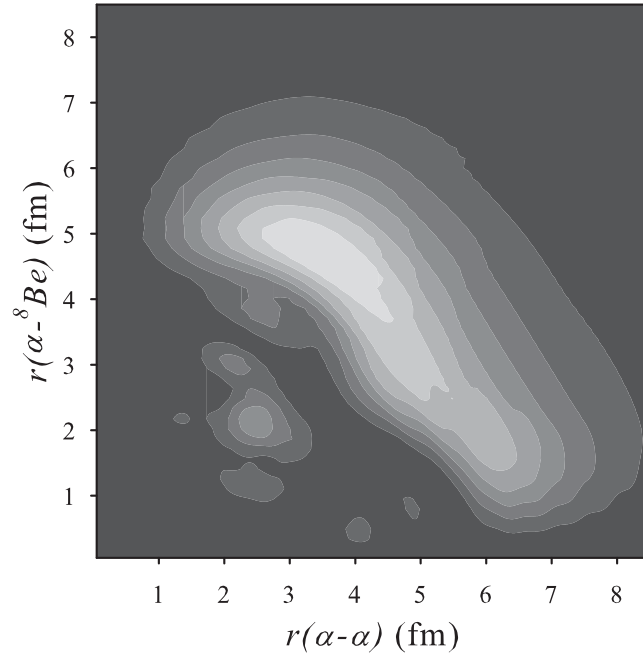


Figure 9: Correlation function for the first  $0^+$  resonance state of  $^{12}\text{C}$  in the coordinate space.

than the weight of the prolate triangular configuration. Our calculations therefore do not agree with other authors advancing a dominant linear structure [30–33].

We display in Fig. 10 the correlation function of the first resonance state in the momentum space. One observes a huge maximum corresponding to relatively slowly moving  $\alpha$ -particles. A small maximum corresponding to faster moving alpha-particles is also present.

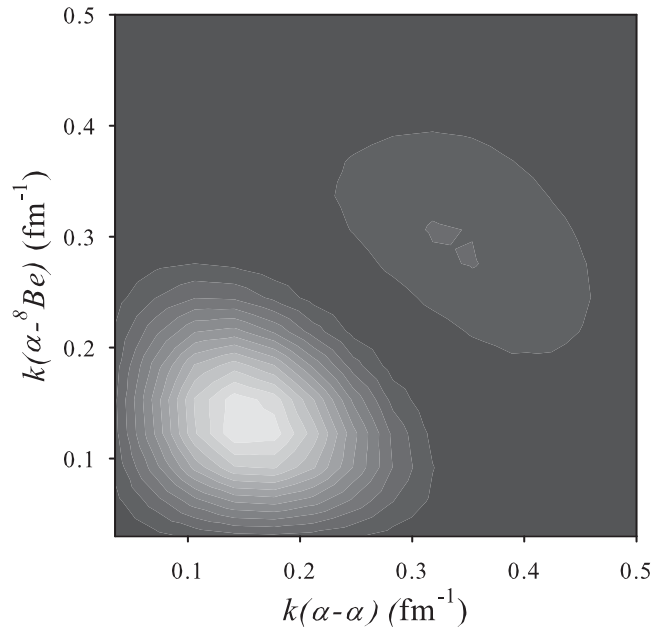


Figure 10: Correlation function for the first  $0^+$  resonance state of  $^{12}\text{C}$  in the momentum space.

Table 8: Bound and resonance states in  $^{12}\text{C}$  obtained with the AMHHB model, compared to CSM results from the literature.

Method Reference $J^\pi$	AMHHB		CSM		CSM	
	Present paper		Arai [17]		Pichler <i>et al.</i> [9]	
	$E$ , MeV	$\Gamma$ , keV	$E$ , MeV	$\Gamma$ , keV	$E$ , MeV	$\Gamma$ , keV
$0^+$	-11.372		-11.37		-10.43	
	0.684	2.78	0.4	< 1	0.64	14
	5.156	534.00	4.7	1000	5.43	920
$2^+$	-8.931		-8.93		-7.63	
	2.775	9.95	2.1	800	6.39	1100
	3.170	280.24	4.9	900		
$4^+$	-3.208		-3.21			
	5.603	0.55	5.1	2000		
$1^-$	3.516	0.21	3.4	200	3.71	360
$3^-$	0.672	8.34	0.6	< 50	1.16	25
	4.348	2.89	7.1	5400	11.91	1690
	5.433	334.90	9.6	400		

### 3.6 Comparison to the literature

We now compare the AMHHB results to the existing literature. We display in Table 8 the AMHHB results together with those of Arai [17] and Pichler *et al.* [9], both obtained by the Complex Scaling Method (CSM). The authors of Ref. [9] use a somewhat different value for the parameter  $u$  of the Minnesota potential and a different oscillator length  $b$ ; because of this, different results are obtained for the bound states.

Comparison with the results of Arai [17] indicates that the AMHHB model leads to resonance states with higher energies and smaller widths than those obtained with the CSM. This can be attributed to the difference of methods and to the different Hilbert spaces. Formally, the Hilbert space of basis functions used by Arai [17] is quite close to the one considered in the AMHHB. Actually, in the present calculations the partial orbital momenta  $l_1$  and  $l_2$  are restricted by the condition

$$L \leq l_1 + l_2 \leq K_{\max}$$

so that, for instance, for the total orbital momentum  $L = 0$ , they run from  $l_1 = l_2 = 0$  to  $l_1 = l_2 = 6$  with  $K_{\max} = 14$ . Arai, on the other hand, restricted himself with  $l_1, l_2 \leq 4$ . In [35, 36, 37] we observed the tendency that the more Hyperspherical Harmonics (thus the more channels) are involved in the calculation, the smaller becomes the resonance energy and width. This tendency is again confirmed by the present AMHHB calculations. Thus some reduction of the width of the resonances observed in our calculations with respect to Arai [17], can be attributed to a larger number of channels in our model.

Comparing the AMHHB results with the Complex Scaling Model calculations of Pichler *et al.* [9], one observes that both yield close results for the first and the second  $0^+$  resonance states.

On the whole one can conclude that there is consistency in the results for resonance properties in all three microscopic models.

### 3.7 Comparison to experiment

We compare the theoretical AMHHB results for  $^{12}\text{C}$  with available experimental data in Table 9.

Table 9: Bound and resonance states in  $^{12}\text{C}$  obtained with the AMHHB model, compared to experiment.

Method Reference $J^\pi$	AMHHB Present paper		Experiment [1]	
	$E$ , MeV	$\Gamma$ , keV	$E$ , MeV	$\Gamma$ , keV
$0^+$	-11.372		-7.2746	
	0.684	2.78	$0.3796 \pm 0.0002$	$(8.5 \pm 1.0) \times 10^{-3}$
	5.156	534.00	$3.0 \pm 0.3$	$3000 \pm 700$
$2^+$	-8.931		$-2.8357 \pm 0.0003$	
	2.775	9.95	$3.89 \pm 0.05$	$430 \pm 80$
	3.170	280.24	$8.17 \pm 0.04$	$1500 \pm 200$
$4^+$	-3.208			
	5.603	0.55	$6.808 \pm 0.015$	$258 \pm 15$
$1^-$	3.516	0.21	$3.569 \pm 0.016$	$315 \pm 25$
	0.672	8.34	$2.366 \pm 0.005$	$34 \pm 5$
$3^-$	4.348	2.89		
	5.433	334.90		

One notices that the first  $0^+$  resonance state (the Hoyle state) appears in the current calculations as a narrow resonance with the energy of 0.684 MeV and the width of 2.7 keV, which is considerably wider than the experimental Hoyle state (about  $8.5 \cdot 10^{-3}$  keV). This contrasts with a generally observed feature of the AMHHB calculations that the calculated widths are significantly less than the respective experimental widths of  $^{12}\text{C}$  resonances. The discrepancies between the theoretical and experimental data have essentially two origins. The first one relates to the choice of the nucleon-nucleon interaction: it was tuned to reproduce the phase shifts and resonance properties for alpha-alpha scattering. As a result, it leads to the overbound  $0^+$  and  $2^+$  states in  $^{12}\text{C}$  and binds the  $4^+$  state. The second one relates to the specific choice of the three-cluster model and corresponding model space, as well as to the method by which energies and widths of resonance states are obtained.

### 3.8 Optimizing the nucleon-nucleon potential

In this paper, we used a Minnesota nucleon-nucleon potential tuned to reproduce phase shifts of  $\alpha$ - $\alpha$  scattering as well as  $^8\text{Be}$  resonances. This however leads to overbound  $0^+$  and  $2^+$  states and a bound  $4^+$  state in  $^{12}\text{C}$ . Moreover, the obtained resonance structure of the  $^{12}\text{C}$  three-cluster continuum deviates from the experimentally observed one which can be also attributed to the specific choice of the semi-realistic nucleon-nucleon potential.

We therefore wish to discuss the dependence of the results on the choice of parameter  $u$  of the potential. To do so, we use different criteria to optimize this parameter. First, we determine a value reproducing the ground state energy of  $^{12}\text{C}$ , followed by an attempt to reproduce the energy and width of the  $0^+$  Hoyle state.

We display in Fig. 11 the ground state energy as a function of the parameter  $u$ , compared to the experiment (dashed line). One observes that the ground state is reproduced with  $u = 0.910$ . One observes a monotonously decreasing linear dependence of the ground state energy on  $u$  within the selected range. For the Hoyle state position and width, the dependency is less trivial as is shown in Fig. 12. One however observes that the value  $u = 0.948$  reproduces the position of the Hoyle state and leads to a close match for its width too.

The correlation functions for the ground state and the Hoyle state obtained with their respective optimal values are very close to those obtained with the value  $u = 0.94$  displayed in Figs. 8 and 9; so, our conclusions remain unaltered.

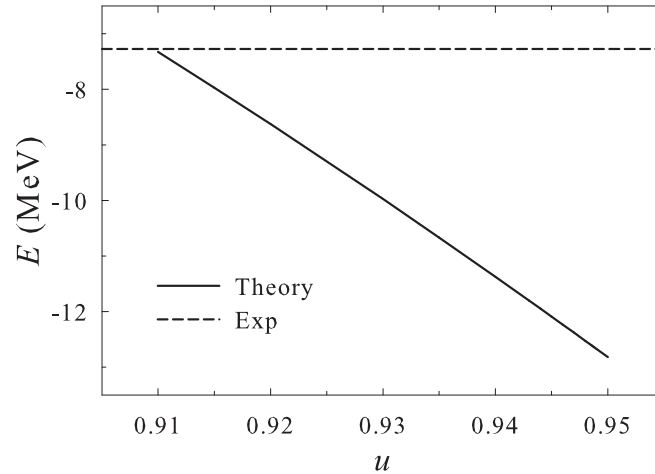


Figure 11: Energy of the ground state as a function of parameter  $u$  of the Minnesota potential.

## 4 Conclusions

In this paper we described the  $^{12}\text{C}$  nucleus with a three-cluster microscopic model.

The model correctly handles the three-cluster continuum, i. e., correctly implements the suitable boundary conditions by using the Hyperspherical Harmonic basis. It leads to the scattering matrix  $S$  in many-channel space, and energies, total and partial widths of resonance states and their corresponding wave functions can be obtained.

It was shown that the obtained resonances of  $^{12}\text{C}$  agree well with those obtained by other methods, and that the lowest resonances are generated by only a few weakly coupled channels leading to narrow resonance states. Partial widths determine the

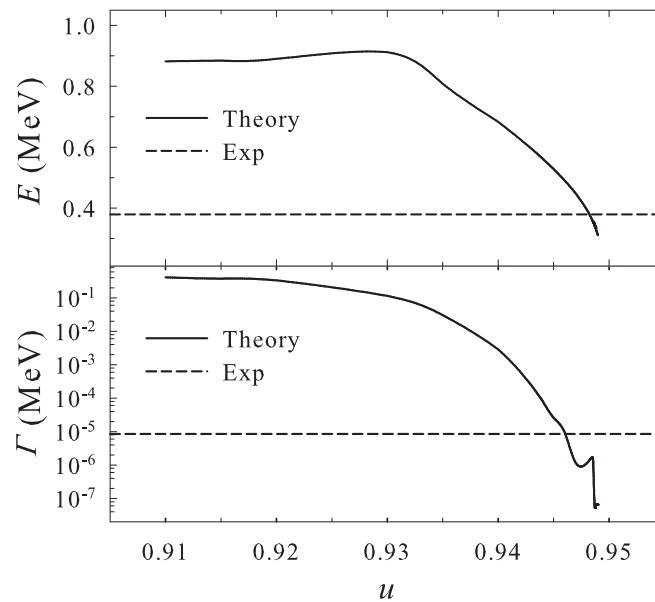


Figure 12: Position and total width of the first  $0^+$  resonance state as a function of parameter  $u$ .



most probable channels for resonance decay. Correlation functions and density distributions reveal the dominant shape of the three-cluster triangle configuration for the lowest bound and resonance states of  $^{12}\text{C}$ . There is no indication of a prominent linear three-cluster structure for resonance states.

It was also shown that it is impossible to fix a unique value for the  $u$  parameter of the Minnesota nucleon-nucleon potential to fit all desired physical properties of  $^{12}\text{C}$  and of the disintegrating  $\alpha$ -particles. However, the qualitative conclusions remained unaltered under a slight adaptation of  $u$ .

As a final conclusion, we can state that the model is consistent with other microscopic models using the Complex Scaling methodology to determine energies and total widths of three-cluster resonance states.

## 5 Acknowledgments

Support from the Fonds voor Wetenschappelijk Onderzoek Vlaanderen (FWO), G0120-08N is gratefully acknowledged. V. S. Vasilevsky is grateful to the Department of Mathematics and Computer Science of the University of Antwerp for hospitality. This work was supported in part by the Program of Fundamental Research of the Physics and Astronomy Department of the National Academy of Sciences of Ukraine.

## References

- [1] F. Ajzenberg-Selove, Nucl. Phys. A **506**, 1 (1990).
- [2] S. I. Fedotov, O. I. Kartavtsev, V. I. Kochkin and A. V. Malykh, Phys. Rev. C **70**, 014006 (2004).
- [3] I. Filikhin, V. M. Suslov and B. Vlahovic, J. Phys. G **31**, 1207 (2005).
- [4] R. Álvarez-Rodríguez, E. Garrido, A. S. Jensen, D. V. Fedorov and H. O. U. Fynbo, Eur. Phys. J. A **31**, 303 (2007).
- [5] R. Álvarez-Rodríguez, A. S. Jensen, D. V. Fedorov, H. O. U. Fynbo and E. Garrido, J. Phys. Conf. Ser. **111**, 012017 (2008).
- [6] R. Álvarez-Rodríguez, A. S. Jensen, E. Garrido, D. V. Fedorov and H. O. U. Fynbo, Phys. Rev. C **77**, 064305 (2008).
- [7] M. Chernykh, H. Feldmeier, T. Neff, P. von Neumann-Cosel and A. Richter, Phys. Rev. Lett. **105**, 022501 (2010).
- [8] R. de Diego, E. Garrido, D. V. Fedorov and A. S. Jensen, Phys. Lett. B **695**, 324 (2011).
- [9] R. Pichler, H. Oberhummer, A. Csótó and S. A. Moszkowski, Nucl. Phys. A **618**, 55 (1997).
- [10] C. Kurokawa and K. Katō, Nucl. Phys. A **738**, 455 (2004).
- [11] Y. Fujiwara, K. Miyagawa, M. Kohno, Y. Suzuki, D. Baye and J.-M. Sparenberg, Nucl. Phys. A **738**, 495 (2004).
- [12] Y. Fujiwara, Y. Suzuki and M. Kohno, Phys. Rev. C **69**, 037002 (2004).
- [13] Y. Fujiwara, M. Kohno and Y. Suzuki, Few-Body Syst. **34**, 237 (2004).
- [14] Y. Fujiwara and H. Nemura, Prog. Theor. Phys. **107**, 745 (2002).

- 
- [15] Y. Fujiwara, K. Miyagawa, M. Kohno, Y. Suzuki, D. Baye and J.-M. Sparenberg, *Phys. Rev. C* **70**, 024002 (2004).
- [16] C. Kurokawa and K. Katō, *Phys. Rev. C* **71**, 021301 (2005).
- [17] K. Arai, *Phys. Rev. C* **74**, 064311 (2006).
- [18] M. Theeten, H. Matsumura, M. Orabi, D. Baye, P. Descouvemont, Y. Fujiwara and Y. Suzuki, *Phys. Rev. C* **76**, 054003 (2007).
- [19] C. Kurokawa and K. Katō, *Nucl. Phys. A* **792**, 87 (2007).
- [20] P. Descouvemont and D. Baye, *Phys. Rev. C* **36**, 54 (1987).
- [21] M. Orabi, Y. Suzuki, H. Matsumura, Y. Fujiwara, D. Baye, P. Descouvemont and M. Theeten, *J. Phys. Conf. Ser.* **111**, 012045 (2008).
- [22] Y. Suzuki, H. Matsumura, M. Orabi, Y. Fujiwara, P. Descouvemont, M. Theeten and D. Baye, *Phys. Lett. B* **659**, 160 (2008).
- [23] P. Descouvemont, *J. Phys. G* **37**, 064010 (2010).
- [24] T. Yoshida, N. Itagaki and K. Katō, *Phys. Rev. C* **83**, 024301 (2011).
- [25] N. Moiseyev, *Phys. Rep.* **302**, 212 (1998).
- [26] Y. K. Ho, *Phys. Rep.* **99**, 1 (1983).
- [27] T. Muñoz-Britton, M. Freer, N. I. Ashwood, T. A. D. Brown, W. N. Catford, N. Curtis, S. P. Fox, B. R. Fulton, C. W. Harlin, A. M. Laird, P. Mumby-Croft, A. S. J. Murphy, P. Papka, D. L. Price, K. Vaughan, D. L. Watson and D. C. Weisser, *J. Phys. G* **37**, 105104 (2010).
- [28] M. Freer, H. Fujita, Z. Buthlezi, J. Carter, R. W. Fearick, S. V. Förtsch, R. Neveling, S. M. Perez, P. Papka, F. D. Smit, J. A. Swartz and I. Usman, *Phys. Rev. C* **80**, 041303 (2009).
- [29] A. I. Baz', *Sov. Phys. JETP* **43**, 205 (1976).
- [30] G. S. Anagnostatos, *Phys. Rev. C* **51**, 152 (1995).
- [31] A. C. Merchant and W. D. M. Rae, *Nucl. Phys. A* **549**, 431 (1992).
- [32] Y. Kanada-En'yo, *Progr. Theor. Phys.* **117**, 655 (2007).
- [33] T. Neff and H. Feldmeier, *Nucl. Phys. A* **738**, 357 (2004).
- [34] V. Vasilevsky, A. V. Nesterov, F. Arickx and J. Broeckhove, *Phys. Rev. C* **63**, 034606 (2001).
- [35] V. Vasilevsky, A. V. Nesterov, F. Arickx and J. Broeckhove, *Phys. Rev. C* **63**, 034607 (2001).
- [36] J. Broeckhove, F. Arickx, P. Hellinckx, V. S. Vasilevsky and A. V. Nesterov, *J. Phys. G* **34**, 1955 (2007).
- [37] V. S. Vasilevsky, F. Arickx, J. Broeckhove and V. N. Romanov, *Ukr. J. Phys.* **49**, 1053 (2004).
- [38] S. Korenov and P. Descouvemont, *Nucl. Phys. A* **740**, 249 (2004).
- [39] A. Damman and P. Descouvemont, *Phys. Rev. C* **80**, 044310 (2009).

- 
- [40] Y. Fujiwara, Y. Suzuki, K. Miyagawa and Michio, *Prog. Theor. Phys.* **107**, 993 (2002).
- [41] Yu. A. Lashko and G. F. Filippov, *Nucl. Phys. A* **826**, 24 (2009).
- [42] W. Zickendraht, *Ann. Phys. (NY)* **35**, 18 (1965).
- [43] J. Nyiri and Ya. A. Smorodinsky, *Yad. Fiz.* **29**, 833 (1979).
- [44] A. V. Nesterov, F. Arickx, J. Broeckhove and V. S. Vasilevsky, *Phys. Part. Nucl.* **41**, 716 (2010).
- [45] D. R. Thompson, M. LeMere and Y. C. Tang, *Nucl. Phys. A.* **286**, 53 (1977).
- [46] A. Sytcheva, F. Arickx, J. Broeckhove and V. S. Vasilevsky, *Phys. Rev. C* **71**, 044322 (2005).
- [47] K. Wildermuth and Y. Tang, *A unified theory of the nucleus*. Vieweg Verlag, Braunschweig, 1977.
- [48] V. Vasilevsky, A. V. Nesterov, F. Arickx and J. Broeckhove, *Phys. Rev. C* **63**, 064604 (2001).